Computational Materials Science 45 (2009) 611–616

Contents lists available at ScienceDirect

Computational Materials Science

journal homepage: www.elsevier.com/locate/commatsci

An extended Mori–Tanaka homogenization scheme for finite strain modeling of debonding in particle-reinforced elastomers

L. Brassart [a,*], H.M. Inglis [b], L. Delannay [a], I. Doghri [a], P.H. Geubelle [c]

[a] Department of Mechanical Engineering, Université catholique de Louvain, 4 Avenue Georges Lemaître, B-1348, Louvain-la-Neuve, Belgium
[b] Department of Mechanical Science and Engineering, University of Illinois at Urbana-Champaign, 1206 West Green Street, Urbana, IL 61801, USA
[c] Department of Aerospace Engineering, University of Illinois at Urbana-Champaign, 104 South Wright Street, Urbana, IL 61801, USA

ARTICLE INFO

Article history:
Received 19 December 2007
Received in revised form 16 June 2008
Accepted 24 June 2008
Available online 13 August 2008

PACS:
81.05.Qk
46.15.-x
02.70.Dh

Keywords:
Micromechanics
Micro–macro modeling
Damage
Cohesive law
Mean-field
Finite elements

ABSTRACT

In the present study, the strength and failure of elastomeric composites are predicted by extending the Mori and Tanaka [T. Mori, K. Tanaka, Acta Metallurgica 21 (1973) 571–574] model from the case of perfectly adherent, linear elastic constituents to the case of nonlinear (hyperelastic) constituents subjected to particle debonding. A finite strain formalism is adopted, and an exponential cohesive zone model is used at the particle–matrix interface. Instead of relying on Eshelby's solution, the isolated inclusion problem is solved numerically using a finite element discretization. The proposed homogenization scheme is applied to a solid propellant in which the particles are much stiffer than the matrix. The analysis is performed in plane strain under axisymmetric tensile loading conditions, and the predictions are compared to reference full-field solutions obtained by finite element simulations on unit cells with periodic boundary conditions. It is demonstrated that the new method yields acceptable predictions until the onset of damage, while dramatically reducing the computational time.

1. Introduction

This paper addresses particle debonding in hyperelastic particulate composites such as solid propellants, explosives and other reinforced elastomers, in which the matrix can be ten thousand times more compliant than the particles. The modeling aims to predict the influence of particle debonding on the load bearing capacity of the composite. The model relies on a cohesive traction–separation law that reproduces experimental observations, according to which decohesion of large particles precedes that of smaller particles [1].

Mori and Tanaka [2] modeled particle-reinforced composites by assuming that each particle behaves as an ellipsoidal inclusion isolated within a fictitious, infinite matrix, seeing the average strain of the real matrix as a far-field strain (see also Benveniste [3]). For linear (thermo-) elastic composites with perfectly bonded interfaces, the strain in the isolated inclusion is uniform and given by Eshelby's seminal work [4]. However, transposing this result to the case of nonlinear hyperelastic composites is not trivial and requires appropriate linearization procedure, see for instance [5–7] and references therein. Particle debonding, if it occurs, is another source of discrepancy with regard to Eshelby's reference solution.

In the mean-field homogenization (MFH) model proposed here, the deformation of the isolated inclusion is computed numerically, using an axisymmetric finite element (FE) discretization. Debonding is modeled by means of a traction–separation law, while the response of individual phases is not linearized (contrarily to conventional mean-field theories). Note that Tan et al. [8] and Inglis et al. [9] adopted the same methodology for the case of linear material response, infinitesimal strains and a bilinear cohesive law [10]. Under these assumptions, they could rely on an analytic solution of the isolated inclusion problem.

From a computational viewpoint, the proposed method is much cheaper than a full-field FE solution of the stress and strain fields throughout a representative volume element (RVE) [11,12]. Indeed, statistically meaningful, full-field predictions require that the model microstructure (i.e. the FE mesh) comprise many particles in a range of different sizes. Full-field predictions are presented here within the framework of the mathematical theory of homogenization (MTH), which links multiple length scales based on asymptotic expansions of solution fields [13]. Here, MTH delivers

* Corresponding author.
E-mail address: laurence.brassart@uclouvain.be (L. Brassart).

0927-0256/$ - see front matter © 2008 Elsevier B.V. All rights reserved.
doi:10.1016/j.commatsci.2008.06.021

reference solutions that the simplified mean-field theory aims to reproduce. We consider only the simplest case of spherical particles and axisymmetric tensile loading in plain strain.

The paper is organized as follows. The problem and the constitutive laws are presented in Section 2. Section 3 details the mean-field procedure whereas Section 4 describes the full-field modeling of the RVE. Numerical predictions are discussed in Section 5.

2. Problem description

Consider a heterogeneous material subjected to the macroscopic deformation gradient $\overline{\boldsymbol{F}}$. The matrix phase ω_0 has an initial volume fraction v_0, and each reinforcing phase ω_I (representing all particles having the same shape, size and material properties) has a volume fraction v_I, satisfying $v_0 + \sum_I v_I = 1$. We aim to determine the overall mechanical response of the composite while accounting for damage evolution.

Although the modeling is not restricted to this special case, individual phases are considered hyperelastic. The constitutive laws are derived from a stored energy function per unit reference volume: $\overline{W}(\boldsymbol{X}, \boldsymbol{C})$, where $\boldsymbol{X}$ is a position vector in the reference configuration and $\boldsymbol{C} = \boldsymbol{F}^{\mathrm{T}} \cdot \boldsymbol{F}$ is the right Cauchy-Green strain tensor. In the compressible case, the hyperelastic potential for the modified Neo–Hookean model is written in terms of I_1, the first invariant of $\mathbf{C}$, and $J = \det(\boldsymbol{F})$ as [14]:

$$\overline{W} = \frac{\mu}{2}(J^{-2/3} I_1 - 3) + \frac{\kappa}{2}(J-1)^2, \tag{1}$$

where $\mu = \frac{E}{2(1+\nu)}$ and $\kappa = \frac{E}{3(1-2\nu)}$, E and ν being Young's modulus and Poisson's ratio, respectively. The second Piola–Kirchhoff stress $\boldsymbol{S}$ is found to be:

$$\boldsymbol{S} = 2\frac{\partial \overline{W}}{\partial \boldsymbol{C}} = \mu J^{-2/3}\left(\mathbf{1} - \frac{1}{3} I_1 \boldsymbol{C}^{-1}\right) + \kappa(J^2 - J)\boldsymbol{C}^{-1}, \tag{2}$$

where $\mathbf{1}$ is the second-order identity tensor.

Debonding at particle/matrix interfaces is modeled by a traction–separation law [13], which relates the displacement jump $\boldsymbol{\chi}$ (also known as the interface opening) to the cohesive traction $\boldsymbol{t}_0$ through:

$$\boldsymbol{t}_0 = \frac{\tilde{t}}{\tilde{\chi}}\hat{\boldsymbol{t}}, \qquad \hat{\boldsymbol{t}} = \beta\boldsymbol{\chi} + (1-\beta)(\boldsymbol{\chi}\cdot\boldsymbol{N})\boldsymbol{N}, \tag{3}$$

where $\boldsymbol{N}$ is the outward unit normal to the boundary of the particle. The effective opening displacement $\tilde{\chi}$ is:

$$\tilde{\chi} = \sqrt{\beta^2 \tilde{\chi}_s^2 + \tilde{\chi}_n^2}, \tag{4}$$

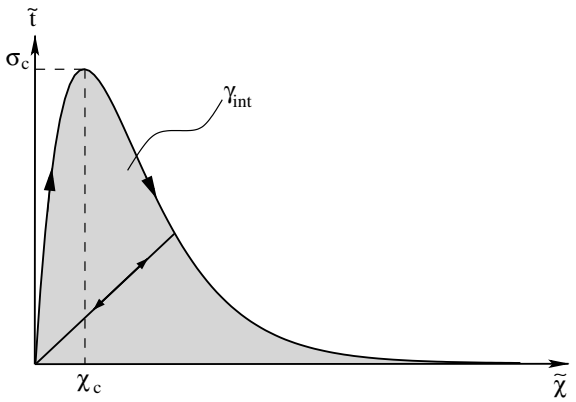

Fig. 1. Exponential traction–separation law showing an unloading path directed towards the origin.

where β assigns different weights to the sliding and normal opening displacements $\tilde{\chi}_s$ and $\tilde{\chi}_n$. In the current study, β is set equal to 1.

The present work adopts an exponential cohesive law:

$$\tilde{t} = \sigma_c \frac{\tilde{\chi}}{\chi_c}\exp\left(1 - \tilde{\chi}/\chi_c\right), \tag{5}$$

where χ_c denotes a reference opening displacement and σ_c is the maximum effective cohesive traction, as shown in Fig. 1. Unloading of the cohesive law is allowed, and directed towards the origin according to:

$$\tilde{t} = \frac{\tilde{t}_{\max}}{\tilde{\chi}_{\max}}\tilde{\chi}, \tag{6}$$

where $\tilde{\chi}_{\max}$ is the maximum opening displacement that has ever been attained during previous loading, and $\tilde{t}_{\max}$ is the corresponding cohesive traction. This feature of the cohesive law is essential since smaller particles often unload during the debonding of larger ones, even when macroscopic loading is monotonic. The interface fracture toughness for the cohesive law (5) is given by $\gamma_{\mathrm{int}} = \int_0^\infty \tilde{t}\,\mathrm{d}\tilde{\chi} = \exp(1)\sigma_c\chi_c$.

3. Simplified modeling based on mean-field homogenization (MFH)

This section is devoted to mean-field modeling of particle debonding. If a displacement $\bar{\boldsymbol{u}} = \overline{\boldsymbol{F}}\cdot\boldsymbol{X}$ is prescribed at the boundary $\partial\omega$ of a volume element ω, it has been shown [15] that the average deformation gradient over the RVE is equal to $\overline{\boldsymbol{F}}$:

$$\langle \boldsymbol{F}\rangle_\omega = v_0\langle \boldsymbol{F}\rangle_{\omega_0} + \sum_I v_I(\langle \boldsymbol{F}\rangle_{\omega_I} + \langle \boldsymbol{F}^{\mathrm{int}}\rangle_{\partial\omega_I}) = \overline{\boldsymbol{F}}, \tag{7}$$

where $\langle \boldsymbol{F}^{\mathrm{int}}\rangle_{\partial\omega_I}$ represents the average deformation gradient over the interfaces around particles ω_I due to debonding:

$$\langle \mathbf{F}^{\mathrm{int}}\rangle_{\partial\omega_I} = \frac{1}{V(\omega_I)}\int_{\partial\omega_I} \boldsymbol{\chi}\otimes\mathbf{N}_I\,\mathrm{d}S, \tag{8}$$

and $V(\omega_I)$ represents the volume of particles I.

In a first-order mean-field model, the macroscopic nominal stress is computed as:

$$\bar{\boldsymbol{P}}^{\mathrm{MF}} = v_0\boldsymbol{P}^0 + \sum_I v_I\boldsymbol{P}^I, \tag{9}$$

where $\boldsymbol{P}^0$ and $\boldsymbol{P}^I$ are estimations of $\langle \boldsymbol{P}\rangle_{\omega_0}$ and $\langle \boldsymbol{P}\rangle_{\omega_I}$ obtained by applying the constitutive laws to $\langle \boldsymbol{F}\rangle_{\omega_0}$ and $\langle \boldsymbol{F}\rangle_{\omega_I}$, respectively. Thus, estimations of the average strains in each material phase are required.

In order to determine $\langle \boldsymbol{F}\rangle_{\omega_I}$ and $\langle \boldsymbol{F}^{\mathrm{int}}\rangle_{\partial\omega_I}$, let us consider that for each reinforcing phase, each particle can be treated as an isolated

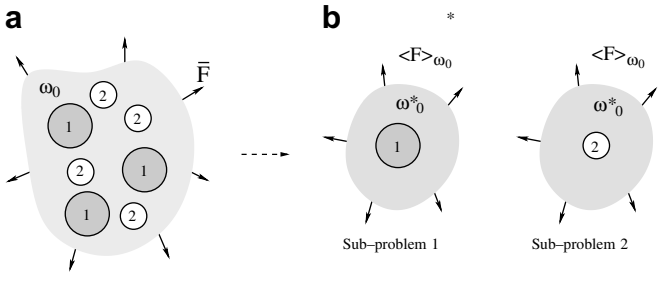

Fig. 2. The original boundary condition problem is subdivided into several isolated inclusion problems, each of them seeing the average strain in the matrix as far-field strain.

inclusion embedded in a fictitious matrix ω_0^*. The RVE is then replaced by several sub-problems, as depicted in Fig. 2. In every sub-problem of domain ω^*, the volume fraction of the inclusion is infinitesimal and – extending the original Mori–Tanaka scheme [2] – the far-field strain imposed on $\partial\omega^*$ corresponds to the average effective deformation gradient in the real matrix $\langle \boldsymbol{F}\rangle_{\omega_0}$ [3]. The displacement field $\boldsymbol{u}(\boldsymbol{X})$ through ω^* is the solution of the following boundary value problem:

$$\begin{cases} \mathrm{DIV}(\boldsymbol{P}) = \boldsymbol{0} \text{ in } \omega^* & \text{(equilibrium)} \\ \bar{\boldsymbol{u}} = (\langle \boldsymbol{F}\rangle_{\omega_0} - \boldsymbol{1})\boldsymbol{X} \text{ on } \partial\omega^* & \text{(displacement B.C.)} \\ \boldsymbol{F} = \boldsymbol{1} + \boldsymbol{\nabla u} & \text{(kinematics)} \\ \text{(constitutive equations and interface behavior)} \end{cases} \tag{10}$$

where DIV($\boldsymbol{P}$) is the divergence of the nominal stress tensor with respect to the reference coordinates. The system of equations (10) is solved by the FE method, permitting the nonlinear material properties and inhomogeneities to be incorporated while reducing computation costs dramatically as compared to a full resolution of the original multiple inclusions problem (see Section 4).

The remainder of this section describes the numerical implementation of this method in the case of equibiaxial (2-D) or hydrostatic (3-D) loading conditions. For simplicity, only circular particle geometries are considered: spherical particles in 3-D or infinitely long fibres in 2-D (plane strain). Each phase ω_I is then characterized by a radius a_I. With lowercase indices taking the values 1, 2 and 3 in 3-D, and 1 and 2 in 2-D, the macroscopic deformation gradient is simply written: $\bar{F}_{ij} = \bar{F}\delta_{ij}$, where δ_{ij} is Kronecker's symbol.

Let us rewrite average quantities taking advantage of the symmetry. The isolated inclusion problem is axially symmetric, and second-order tensors become diagonal. Hence, integrating the deformation gradient over each particle domain and around each interface yields:

$$(\langle F\rangle_{\omega_\mathrm{I}})_{ij} = \left(1 + \frac{u_\mathrm{r}^\mathrm{I}(a_\mathrm{I})}{a_\mathrm{I}}\right)\delta_{ij} \qquad \text{and} \qquad (\langle F^\mathrm{int}\rangle_{\omega_\mathrm{I}})_{ij} = \frac{[u_\mathrm{r}]_\mathrm{I}}{a_\mathrm{I}}\delta_{ij}, \tag{11}$$

where $u_\mathrm{r}^\mathrm{I}(a_\mathrm{I})$ is the radial displacement in the particle at $r = a_\mathrm{I}$, and $[u_\mathrm{r}]_\mathrm{I} = \tilde{\chi}$ is the radial opening displacement. It is deduced from the previous considerations together with (7) that the average deformation gradient in the matrix is also diagonal:

$$(\langle F\rangle_{\omega_0})_{ij} = F^0\delta_{ij}. \tag{12}$$

Therefore, the phase strains are fully determined by the radial displacement in the particles at $r = a_\mathrm{I}$ and by the radial displacement jump $[u_\mathrm{r}]_\mathrm{I}$.

Assuming infinitesimal strains and linear elastic behavior of the (very rigid) particles, the stress field inside the particles is uniform: $P_{ij}^\mathrm{I} = \sigma_\mathrm{I}^\mathrm{int}\delta_{ij}$, with $\sigma_\mathrm{I}^\mathrm{int} = \tilde{t}$ around interfaces I. In 2-D, the radial displacement of the particle at $r = a_\mathrm{I}$ is readily found analytically using Airy's functions (see for instance [14]):

$$\frac{E_\mathrm{I}}{(1+\nu_\mathrm{I})(1-2\nu_\mathrm{I})}\frac{u_\mathrm{r}^\mathrm{I}(a_\mathrm{I})}{a_\mathrm{I}} = \sigma_\mathrm{I}^\mathrm{int}. \tag{13}$$

Hence, the displacement field $\boldsymbol{u}(r) = u_\mathrm{r}(r)\boldsymbol{e}_\mathrm{r}$ must be computed numerically only within the fictitious matrix of outer radius b, with $\frac{a_\mathrm{I}}{b} \ll 1$. The domain ω_0^* is subject to mixed boundary conditions: displacements are imposed at $r = b$:

$$u_\mathrm{r}(b) = b(F^0 - 1), \tag{14}$$

while the cohesive traction $\boldsymbol{t}_0$ is applied at the particle–matrix interface:

$$\boldsymbol{P}\cdot(-\boldsymbol{e_r}) = \boldsymbol{t}_0. \tag{15}$$

The principle of virtual work states that:

$$\int_{\omega_0^*} \boldsymbol{P} : \nabla(\boldsymbol{v})\mathrm{d}V - \int_{\mathrm{r}=a_\mathrm{I}} \boldsymbol{t}_0\cdot\boldsymbol{v}\mathrm{d}S = 0 \tag{16}$$

for all admissible displacements $\boldsymbol{v} \in [H^1]$ satisfying $\boldsymbol{v} = \boldsymbol{0}$ on $r = b$, where $[H^1]$ is the Sobolev space for the 2-D or 3-D problem. Eq. (16) serves as the basis for an axisymmetric (1-D) finite element solution.

In the 2-D axisymmetric setting, Eq. (16) reduces to:

$$\int_{a_\mathrm{I}}^{b}\left(P_{\mathrm{rr}}\frac{\partial v_\mathrm{r}}{\partial r}r + P_{\theta\theta}v_\mathrm{r}\right)\mathrm{d}r = -a_\mathrm{I}\sigma_1^\mathrm{int}v_\mathrm{r}(a_\mathrm{I}). \tag{17}$$

In 3-D, integration of Eq. (16) using spherical coordinates yields:

$$\int_{a_\mathrm{I}}^{b}\left(P_{\mathrm{rr}}\frac{\partial v_\mathrm{r}}{\partial r}r^2 + (P_{\phi\phi}+P_{\theta\theta})v_\mathrm{r}\right)\mathrm{d}r = -a_\mathrm{I}^2\sigma_\mathrm{I}^\mathrm{int}v_\mathrm{r}(a_\mathrm{I}), \tag{18}$$

while the analytical displacement of the particle at $r = a_\mathrm{I}$ is analytically found to be:

$$\frac{E_\mathrm{I}}{1-2\nu_\mathrm{I}}\frac{u_\mathrm{r}^\mathrm{I}(a_\mathrm{I})}{a_\mathrm{I}} = \sigma_\mathrm{I}^\mathrm{int}. \tag{19}$$

Eq. (17) in 2-D (or (18) in 3-D) is discretized over N elements using linear shape functions. The N equations (per phase) are coupled to Eq. (13) (or (19) in 3-D), and to Eq. (7), which links the strain averages in the different phases to the macroscopic strain. A total of $N_\phi(N+1)+1$ nonlinear equations is obtained, with N_ϕ the number of reinforcing phases. The system is solved using the Newton–Raphson scheme.

4. Full-field FE modeling based on the mathematical theory of homogenization (MTH)

This section describes the MTH-based FE method providing reference results for the verification of the MFH approach presented in Section 3. The mathematical theory of homogenization [16], extended to the case of finite deformations with cohesive failure in [13], is represented schematically in Fig. 3. It is based on an asymptotic expansion of the displacement field,

$$\boldsymbol{u}(\boldsymbol{X},\boldsymbol{Y}) \approx {}^0\boldsymbol{u}(\boldsymbol{X}) + \xi\,{}^1\boldsymbol{u}(\boldsymbol{X},\boldsymbol{Y}) + \text{h.o.t.}, \tag{20}$$

where $\boldsymbol{X}$ represents the undeformed configuration at the macroscale, $\boldsymbol{Y}$ the undeformed configuration at the microscale, and ξ the asymptotic scaling parameter ($\boldsymbol{X} = \xi\boldsymbol{Y}$). The macroscopic displacement term ${}^0\boldsymbol{u}(\boldsymbol{X})$ is continuous, while discontinuities and heterogeneities are modeled by the fluctuating displacement term ${}^1\boldsymbol{u}(\boldsymbol{X},\boldsymbol{Y})$. The deformation gradient can then be written

$$\boldsymbol{F} = \boldsymbol{1} + \nabla_{\boldsymbol{X}}^0\boldsymbol{u} + \nabla_{\boldsymbol{Y}}^1\boldsymbol{u} = \bar{\boldsymbol{F}} + \tilde{\boldsymbol{F}}, \tag{21}$$

with the macroscopic deformation gradient $\bar{\boldsymbol{F}} = \boldsymbol{1} + \nabla_{\boldsymbol{X}}^0\boldsymbol{u}$ and the microscale deformation gradient $\tilde{\boldsymbol{F}} = \nabla_{\boldsymbol{Y}}^1\boldsymbol{u}$. On the microscale, we solve the equation of equilibrium for the fluctuating displacement field ${}^1\boldsymbol{u}$

$$\frac{1}{|\Theta_0|}\int_{\Theta_0}\boldsymbol{S} : \boldsymbol{F}^\mathrm{T}\nabla_{\boldsymbol{Y}}\delta^1\boldsymbol{u}\mathrm{d}\Theta_0 + \frac{1}{|\Theta_0|}\int_{S_0}\boldsymbol{t}_0\cdot[\delta^1\boldsymbol{u}]\mathrm{d}S = 0, \tag{22}$$

with $[{}^1\boldsymbol{u}] = \boldsymbol{\chi}$ and the imposed macroscopic deformation gradient having the effect of a loading term.

The periodic domain Θ is discretized with linear 3-noded volumetric elements and 4-noded cohesive elements. Eq. (22) is solved using a fully implicit formulation with a Newton–Raphson procedure.

The macroscopic stress $\bar{\boldsymbol{P}}$ is then computed as the "exact" volume average of the nominal stress over the RVE:

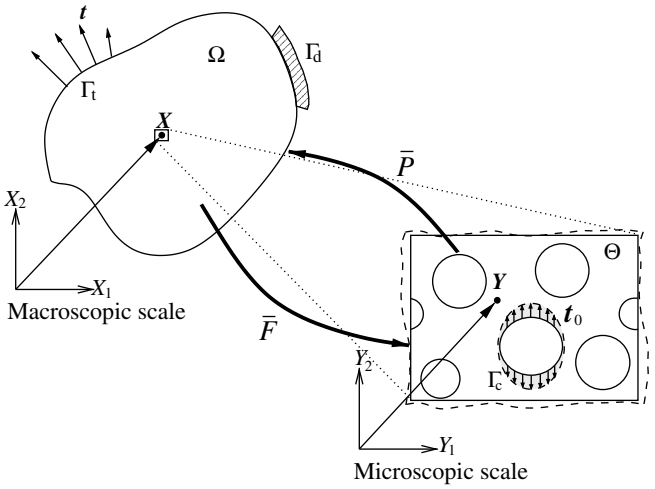

Fig. 3. Schematic representation of the multiscale problem with $\bar{\boldsymbol{P}}$ and $\bar{\boldsymbol{F}}$ denoting the macroscopic nominal stress and deformation fields, respectively. Heterogeneities and discontinuities are visible only at the microscale. $\boldsymbol{t}_0$ represents the cohesive traction vector acting along the particle–matrix interface Γ_c.

$$\overline{\boldsymbol{P}}^{\boldsymbol{FE}} = \langle \boldsymbol{P} \rangle_{\omega} \tag{23}$$

where the nominal stress $\boldsymbol{P}$ is computed as: $\boldsymbol{P} = \boldsymbol{S} \cdot \boldsymbol{F}^{\mathrm{T}}$.

5. Numerical results

In this section, approximate results provided by the MFH approach (Section 3) are compared to full-field FE predictions (Section 4) in 2-D meshes using periodic boundary conditions. Volumetric material properties are the following: $E^{\mathrm{m}} = 2.4$ MPa, $\nu^{\mathrm{m}} = 0.4$ for the hyperelastic matrix, and $E^{\mathrm{p}} = 30$ GPa, $\nu^{\mathrm{p}} = 0.1433$ for the hard particles. The cohesive strength σ_c is set to 0.5 MPa. Taken together, these properties ensure that debonding occurs in the large strain regime.

We consider first a unit cell containing a single particle subjected to 2-D axisymmetric tensile loading. Fig. 4 shows the result of the comparison for different values of the characteristic opening displacement χ_c, for a composite with 20% of particles of radius 10 μm. It clearly appears that the Mori–Tanaka solution correctly captures the initial slope and damage initiation. However, the two solutions diverge substantially after the debonding, with an overestimation of the macroscopic stress by the mean-field approach. A similar behavior of the Mori–Tanaka solution is also observed in Fig. 5 which shows the macroscopic response resulting from both approaches for different volume fractions, with $\chi_c = 1$ μm.

Random arrangements of particles are investigated in Fig. 6, showing results from cells containing 1, 6, and 10 particles, respectively. The macroscopic responses for all three cases agree with each other and with the Mori–Tanaka predictions. Unit cells containing more particles give rise to an earlier onset of strain localization. At 20% total strain, the six particle cell still has nearly uniform failure around each particle, while the 10 particle case already shows marked loss of axisymmetry. This is correlated to the localization process: interactions between particles are more pronounced at some specific points of the interface. The instability of the loading conditions at the interface, coupled with the sharp cohesive law, lead to rapid failure of the portion of the interface which was initially perturbed. This effect was reported in [9] for similar comparisons in the small strain regime.

The size effect due to debonding is predicted by the mean-field approach, as shown in Fig. 7. Two particle sizes are considered,

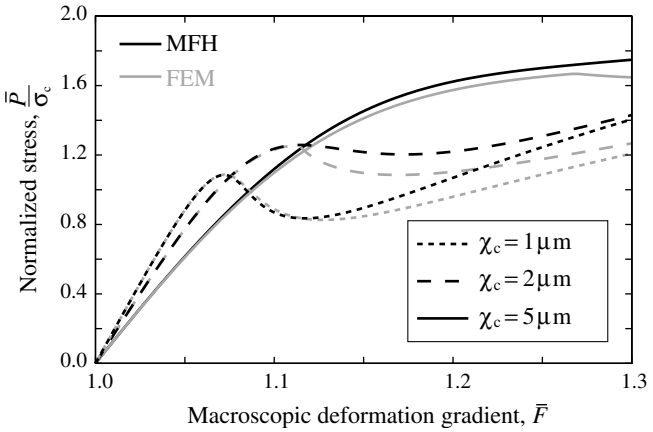

Fig. 4. Comparison between the macroscopic constitutive curves obtained by mean-field homogenization (MFH) and finite element analysis (FEM) for different values of the critical opening displacement; $\nu = 0.2$, $a = 10$ μm.

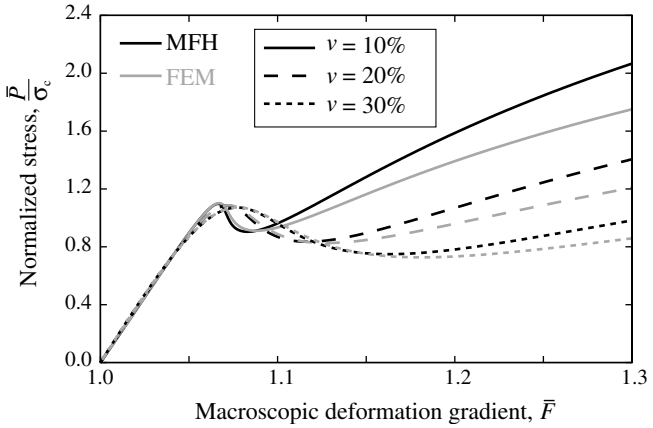

Fig. 5. Effect of particle volume fraction on the macroscopic stress–strain responses from mean-field homogenization (MFH) and finite element analysis (FEM); $\chi_c = 1$ μm, $a = 10$ μm.

with volume fractions ν_1 and ν_2, keeping the radius of large particles and the total volume fraction constant: $a_1 = 20$ μm and $\nu_1 = \nu_2 = 10\%$, for several radii of small particles. Results are compared with the response of the composite with large particles only, $a_2 = a_1 = 20$ μm. Here, χ_c is set equal to 2 μm. As expected, the debonding of large particles precedes the debonding of small ones. Moreover, the reinforcing role of small particles during debonding of large ones clearly appears in this figure.

6. Conclusions

The proposed MFH scheme is based on a numerical resolution of the isolated inclusion problem. In this way, particle debonding can be addressed using a traction–separation law which reproduces the experimentally observed size effect. Predictions are verified against FE simulations performed on periodic unit cells containing several particles.

The results from the two solution methodologies agree with each other until the onset of failure in the large strain domain (10% of deformation). Particle clustering and the associated stress concentrations influence the onset of damage (Fig. 6). Overlooking this is obviously inherent to any mean-field approach. The MFH method also fails to capture the macroscopic strength after debonding. The inability of such method to apprehend a porous matrix is actually common in first-order homogenization schemes, as al-

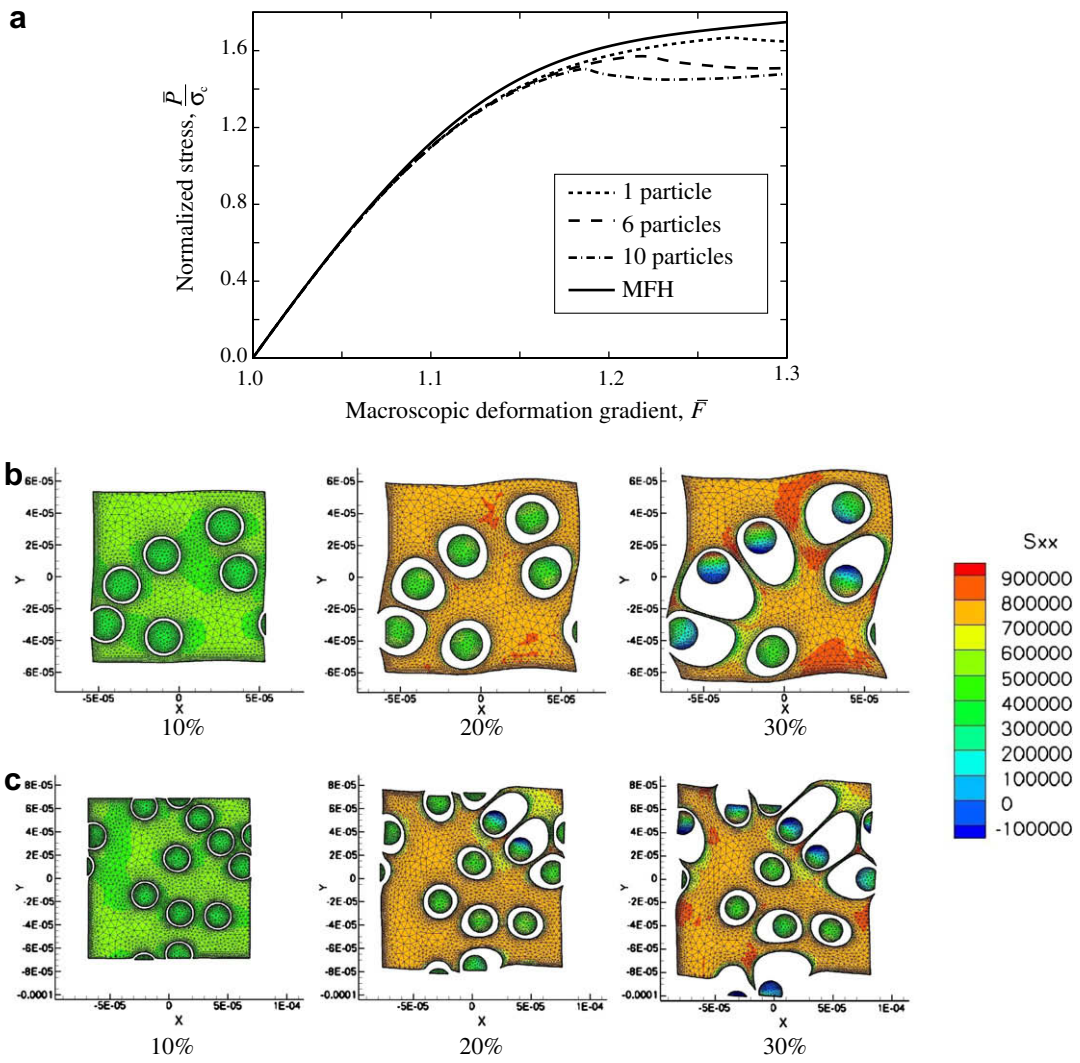

Fig. 6. Effect of unit cell size on (a) the macroscopic constitutive response and (b) and (c) the microscale response for packs containing 6 and 10 particles, respectively. In (b) and (c) the stress field S_{11} is plotted on the deformed shape at total deformation $\bar{F} - 1$ of 10%, 20% and 30%; $\nu = 0.2$, $a = 10$ μm, $\chi_c = 5$ μm.

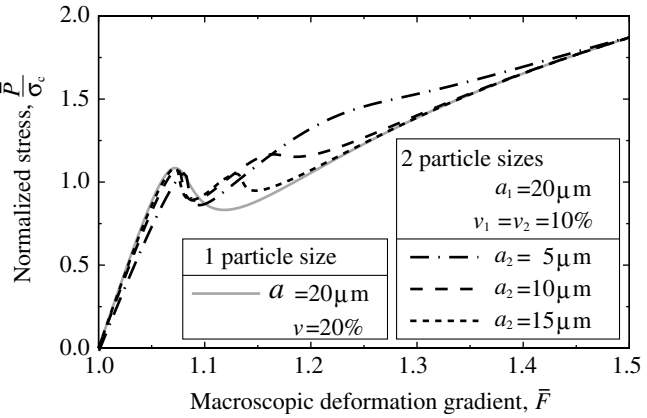

Fig. 7. Macroscopic response of the composite from mean-field homogenization for two different sizes of particles, with the response for a single particle solution shown as a solid line for reference; $a_1 = 20$ μm, $v_1 = v_2 = 10\%$, $\chi_c = 2$ μm.

ready reported in [5,17]. Indeed, first-order schemes assume that the average stress in each phase may be related to the average strain through the local constitutive law. In reality, the effective behavior of porous materials strongly depends on heterogeneities in the local stress field of the matrix. These two shortcomings of the MFH method are thus observed even in the absence of a linearization procedure. Nevertheless, the MFH method provides useful approximate predictions of the influence of microstructural parameters on the debonding process.

The method has been presented in the case of axisymmetric, plane strain loading conditions for hyperelastic composites. Extending the scheme to more general microstructures (e.g. non-spherical inclusions), material laws (e.g. elasto-plasticity) or loading conditions is under way. The development of a second-order instead of first-order MFH method will also be attempted, which should enable to account for intra-phase fluctuations of the stress and strain fields.

Acknowledgements

L. Brassart and L. Delannay are mandated by the National Fund for Scientific Research (FNRS, Belgium). H. M. Inglis and P. H. Geubelle acknowledge the support of the Center for Simulation of Advanced Rockets (CSAR) under Contract Number B523819 by the US Department of Energy.

References

[1] P. Rae, H.T. Goldrein, S.J.P. Palmer, J.E. Field, A.L. Lewis, Proceedings of the Royal Society of London A 458 (2002) 743–762.
[2] T. Mori, K. Tanaka, Acta Metallurgica 21 (1973) 571–574.
[3] Y. Benveniste, Mechanics of Materials 6 (1987) 147–157.
[4] J.D. Eshelby, Proceedings of the Royal Society of London A 241 (1957) 376–396.
[5] A. Rekik, F. Auslender, M. Bornert, A. Zaoui, International Journal of Solids and Structures 44 (2007) 3468–3496.
[6] I. Doghri, A. Ouaar, International Journal of Solids and Structures 40 (2003) 1681–1712.
[7] J.L. Chaboche, P. Kanouté, A. Roos, International Journal of Plasticity 21 (2005) 1409–1434.
[8] H. Tan, Y. Huang, C. Liu, P.H. Geubelle, International Journal of Plasticity 21 (2005) 1890–1918.
[9] H.M. Inglis, P.H. Geubelle, K. Matouš, Y.H. Tan, Mechanics of Materials 39 (2007) 580–595.
[10] H. Tan, C. Liu, Y. Huang, P.H. Geubelle, Journal of the Mechanics and Physics of Solids 53 (2005) 1892–1917.
[11] K. Matouš, P.H. Geubelle, Computer Methods in Applied Mechanics and Engineering 196 (2006) 620–633.
[12] J. Segurado, J. Llorca, Acta Materialia 53 (2005) 4931–4942.
[13] K. Matouš, P.H. Geubelle, International Journal for Numerical Methods in Engineering 65 (2006) 190–223.
[14] I. Doghri, Mechanics of Deformable Solids: Linear and Nonlinear, Analytical and Computational Aspects, Springer, 2000.
[15] S. Govindjee, J. Simo, Journal of the Mechanics and Physics of Solids 39 (1991) 87–112.
[16] A. Bensoussan, J.L. Lions, G. Papanicolaou, Asymptotic Analysis for Periodic Structures, North-Holland, 1978.
[17] R. Masson, M. Bornert, P. Suquet, A. Zaoui, Journal of the Mechanics and Physics of Solids 48 (2000) 1203–1227.